Size distribution of gel and fluid clusters in DMPC/DSPC lipid bilayers. A Monte Carlo simulation study

ARTICLE *in* THE JOURNAL OF PHYSICAL CHEMISTRY B · OCTOBER 2001

Impact Factor: 3.3 · DOI: 10.1021/jp012355q

2 AUTHORS:

Ekaterina Michonova
Erskine College
25 PUBLICATIONS **179** CITATIONS
SEE PROFILE

Istvan Sugar
Icahn School of Medicine at Mount Sinai
80 PUBLICATIONS **1,416** CITATIONS
SEE PROFILE

Size Distribution of Gel and Fluid Clusters in DMPC/DSPC Lipid Bilayers. A Monte Carlo Simulation Study†

Ekaterina I. Michonova-Alexova and István P. Sugár*

Departments of Biomathematical Sciences and Physiology/Biophysics, Mount Sinai School of Medicine at New York University, One Gustave L. Levy Place, New York, New York 10029

Received: June 20, 2001; In Final Form: August 2, 2001

Proteins and lipid components are organized into domains in many biological membranes. With different experimental techniques vastly different cluster sizes have been measured in an equimolar mixture of a DMPC/DSPC two-component lipid bilayer: very small ones in the nanometer range and very large ones of size comparable with the size of the bilayer. In this paper the lateral distribution of gel and fluid lipid molecules in a DMPC/DSPC bilayer is simulated by using a two-state, Ising type model with the application of Monte Carlo methods. The same model has been able to predict the excess heat capacity curves, FRAP threshold temperatures, average coherence length between DSPC clusters, and the fractal dimension of gel clusters, in agreement with the respective experimental data. In this work, similarly to the experimental results, the calculated equilibrium distributions of cluster size show that, between the onset temperature of the gel-to-fluid transition and the percolation threshold temperature of the gel clusters, nanometer size gel clusters coexist with a gel cluster of size comparable to the bilayer's size itself. The calculated upper bound for the size of the small clusters, 8 ± 1.5 nm is very close to the experimental estimate of 10 nm. More than one large gel clusters might be present in the case of nonequilibrium lateral distributions. By means of the calculated temperature dependence of three different cluster size averages we can get insight into the process of cluster growth.

I. Introduction

Biological membranes are complex systems, composed of a large number of different lipids and proteins. Until recently, functional importance was attributed mainly to the membrane proteins, while the lipids were thought to provide a structureless matrix, a natural environment for the macromolecules. However, it was shown recently that the lipid bilayer in the cell membranes has a distinct static and dynamic structural organization on a small scale, which involves formation of lipid domains.[1,2] Since lateral diffusion of membrane components is obstructed in the gel domains the functionally significant in-plane chemical reactions can take place only in the fluid regions. For this reason, it is of critical importance to study the lateral organization of lipid domains. Domains may affect gene expression,[6] the activity of enzymes and receptors bound to the membrane[3] and may result in morphological changes at the cell surface.[5]

To understand the functional role of lipid domains in the real biological membranes, model membranes of lipid mixtures have been thoroughly studied for more than two decades. The thermodynamic parameters of DMPC/DSPC bilayers have been examined experimentally by a number of methods such as differential scanning calorimetry (DSC),[7,8] dilatometry,[9] neutron scattering,[10] NMR,[11,12] ESR,[13] Raman spectroscopy,[14] and Fourier transformed infrared spectroscopy.[15] The structural characteristics of the fluid and gel coexistence region have been examined experimentally by using fluorescence recovery after photobleaching (FRAP),[16,17] fluorescence spectroscopy,[18] and electron spin resonance (ESR)[13] spectroscopy. These studies have established that DMPC and DSPC form nonideal mixtures; i.e., there is a broad gel−fluid coexistence region in the phase diagram of this system. The positive deviation from ideality implies that the minor phase forms small clusters in the continuum of the major phase.[19] For many years only indirect detection of these small clusters was possible.[13,20] Recently, Gliss et al.[21] were able to measure the most frequent center-to-center distance between DSPC clusters in a fully hydrated, equimolar mixture of DMPC/DSPC multilayers by means of neutron diffraction, and found an upper limit of 10 nm for the average linear size of the gel clusters. In similar conditions, more than 3 orders of magnitude larger gel clusters were visualized by fluorescence microscopy[22] in giant unilamellar vesicles (GUV) of equimolar DMPC/DSPC mixture. Only one or a small number of these large clusters were observed in each GUV, and their size was comparable with the size of the vesicle. It is important to note that small clusters from 10 to 50 nm were visualized by using atomic force microscopy on a supported layer of DMPC/DSPC bilayer. In these measurements, however, clusters smaller than 10 nm are below the resolution (personal communication with Drs. Kay Yee Lee and Adrian Muresan) and the mica−lipid interaction hinders the attainment of the equilibrium distribution.[38]

DMPC/DSPC mixtures have been investigated theoretically by the phenomenological theory of regular fluids,[23−25] by mean-field theory of two-component mixtures,[19] and by the Landau theory of phase transitions.[26,27] The above phenomenological methods were unable to give information about the lateral distribution of the bilayer components. Monte Carlo methods have been used to simulate the lateral distribution of the

† Abbreviations: DMPC, dimyristoylphosphatidylcholine; DSC, differential scanning calorimetry; DSPC, dipalmitoylphosphatidylcholine; ESR, electron spin resonance; FRAP, fluorescence recovery after photobleaching; GUV, giant unilamellar vesicle; NMR, nuclear magnetic resonance.

* Corresponding author. Phone (212) 241-8110. Fax (212) 860-4630. E-mail: sugar@camelot.mssm.edu.

10.1021/jp012355q CCC: $20.00
Published on Web 09/27/2001

components in the pure gel or fluid phase regions[28] and the distribution of the gel and fluid state molecules in the gel−fluid mixed phase region of DMPC/DSPC bilayers.[29−31] The advantage of the Monte Carlo method is that both measurable and currently unmeasurable properties of the system can be obtained from the simulations.

In the present work a two-state two-component Ising type model of a DMPC/DSPC bilayer[31] that is in thermal equilibrium with the surrounding was used. This model describes the gel-to-fluid transition as a continuous transition through equilibrium states; i.e., the system is above the critical point. It has been able to predict the following macroscopic and microscopic membrane properties in agreement with the respective experimental data: the excess heat capacity curves,[35] FRAP threshold temperatures,[31] the fractal dimension of gel clusters,[39] and the most frequent center-to-center distance of DSPC clusters.[39] Three types of equilibrium distributions of the size of fluid and gel clusters were simulated: including all the clusters, the largest cluster in each snapshot, and all the clusters but the largest ones. The cluster size distributions and averages were calculated at different temperatures and DMPC/DSPC mole fractions. The temperature dependence of these cluster size averages was utilized to gain insight into the process of cluster growth.

II. Methods

II.A. Lattice Model of DMPC/DSPC Bilayers. A two-state model of a two-component DMPC/DSPC lipid bilayer was utilized. The detailed description of the model can be found elsewhere.[31,35] In this section only a brief and qualitative description of the model is given. By assuming bilayer symmetry, only a single monolayer of the two-component lipid bilayer was modeled as a triangular lattice of N points. Periodic boundary conditions were applied in order to eliminate the effects of the lattice edges[32] and also to reduce the number of the model parameters. [When the model was fitted to a limited number of calorimetric data, the strategy of consecutive parameter estimation was utilized to get a robust set of model parameters (see the Determination of Model Parameters section and Table 1 in ref 31).] All acyl chains of the first (DMPC) and second components (DSPC) were located at the lattice points, each of them being in either one of two possible states, gel (g) or fluid (f). Pairs of nearest neighbor acyl chains were linked together to form phospholipid molecules. There were $N_1/2$ DMPC and $N_2/2$ DSPC molecules in the lattice, where $N_1 + N_2 = N$. Every lattice configuration can be uniquely described by a square matrix **S** and a connection vector **c**, both composed of N elements. Each one of the **S** matrix elements can take values 1, 2, 3, or 4, corresponding to the DMPC acyl chain in the gel state, the DSPC acyl chain in the gel state, the DMPC acyl chain in the fluid state, and the DSPC acyl chain in the fluid state, respectively, while the ith element of the connection vector, c_i, defines the location of the acyl chain covalently attached to the acyl chain at the ith lattice point. Calculating the energy of a configuration, we summed up all the intra- and interchain energies. The intra- and interchain energies depend on the type and state of the respective chain or pair of interacting chains and is independent of the position and orientation of the rotational isomers in the acyl chain. Only nearest-neighbor interactions have been considered between the acyl chains since they are short-range van der Waals interactions. The degeneracy of the intrachain energy depends on the type and state of the acyl chains. Any possible changes in the number of lipid molecules and in the bilayer volume due to the gel-to-fluid transition have been neglected.

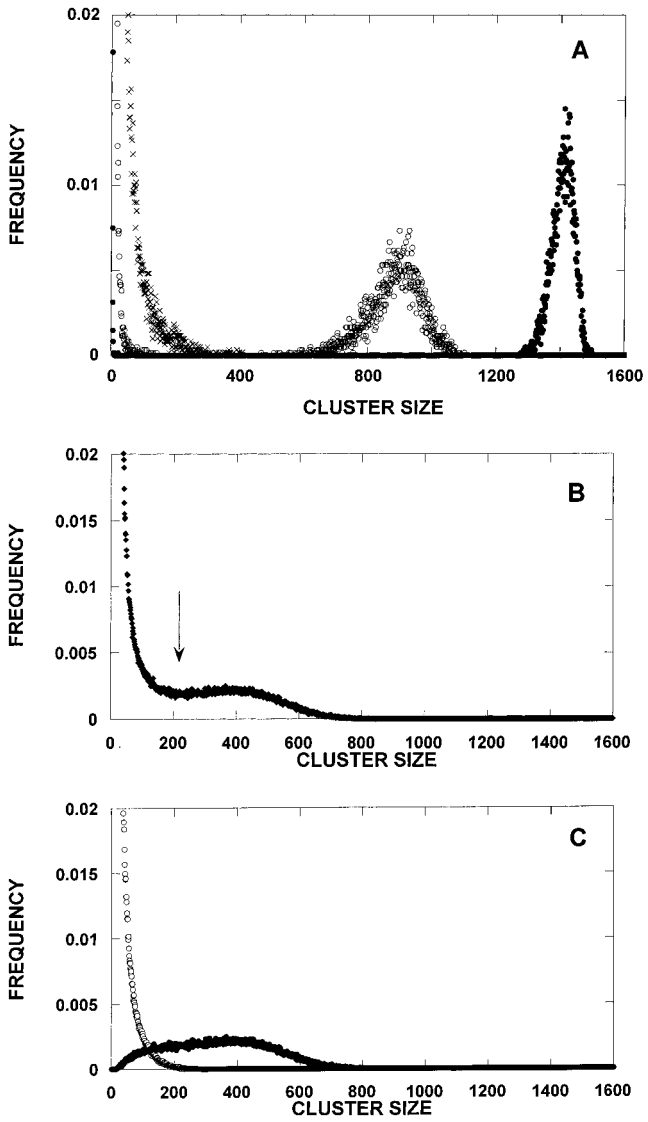

Figure 1. Size distributions of fluid clusters in the DMPC/DSPC (70/30) mixture. (A) Unimodal distribution of all the fluid clusters, $P_{all}(i)$, at $T = 300$ K (cross). Bimodal distributions of all the fluid clusters at $T = 305$ K (open circle) and $T = 314$ K (closed circle). (B) Distribution of all the fluid clusters at $T = 302$ K. The location of the faint minimum, i_{min}, separating the "small" clusters from the "large" ones, is marked by an arrow. (C) Distribution of the largest fluid cluster of each snapshot, $P_{la}(i)$ (closed circle), and of the remaining fluid clusters, $P_{\bar{la}}(i)$ (open circle), at $T = 302$ K. Number of Monte Carlo cycles: 120 000. Number of equilibration cycles: 6000. Lattice size: 40 × 40. Frequency: the average number of clusters of a certain size in a snapshot.

II.B. Steps in the Monte Carlo Simulations. Thermal fluctuations can be simulated in the model of DMPC/DSPC lipid bilayer by means of Monte Carlo methods. The steps of the Monte Carlo simulation have been described in detail before.[31] Each simulation started from either all gel or all fluid state and initially the molecules were similarly oriented. During the simulation trial configurations were generated in three different ways. *First*, a trial configuration was generated by changing the state of a randomly selected acyl chain from gel to fluid, or from fluid to gel. *Second*, two randomly selected molecules of different lipid components were exchanged. *Third*, a pair of nearest neighbor chains was picked randomly. If these two chains belonged to two different molecules and their four chains were located on the nodes of a rhombus, then one of the chains and the chain on the opposite node were exchanged. This

elementary step resulted in a rotation of the molecules by ±60°. Each trial configuration was accepted or rejected according to the Metropolis criterion.[33] A series of such trial steps is essentially a Markov chain, leading eventually to equilibrium distribution of the molecules. The Markov chain can be divided into Monte Carlo cycles. During each Monte Carlo cycle, the system has the opportunity to realize all of its configurations once. In our simulations, each Monte Carlo cycle consisted of the following elementary steps of trial configuration generation: $2N$ elementary steps of local state alterations, followed by N_1 (or N_2 if $N_2 > N_1$) exchange steps and $4N/3$ reorientation steps. [During N consecutive local state alteration trials each lattice point has one opportunity (in average) to change its state and the system to realize any of the 2^N configurations of gel/fluid states.] At the end of each Monte Carlo cycle the state of each acyl chain was altered from gel to fluid or from fluid to gel. This nonphysical trial state generation was used to accelerate the attainment of the equilibrium distribution.[34] To calculate different cluster size distributions and averages, the snapshot was analyzed at the end of each Monte Carlo cycle by using the cluster counting program of Binder and Stauffer.[40]

II.C. Calculating Size Distributions and Averages of "Small" and "Large" Clusters. By using the model described above, we determined the size distribution of all clusters, $P_{all}(i)$, at different temperatures and mixing ratios. After the equilibrium was attained, the snapshot was analyzed at the end of each Monte Carlo cycle. The size of each cluster was determined in the snapshot in order to construct the cluster size distribution. The size of a (gel or fluid) cluster is defined by the number of lattice points in the cluster. The simulations resulted in either unimodal or bimodal distributions, depending on the temperature and on the mixing ratio (see Figure 1A,B). The unimodal distribution refers only to "small" clusters, while the bimodal shows the distribution of both "small" and "large" clusters. Calculating the average cluster size of the "small" and "large" clusters ($\langle i\rangle_s$ and $\langle i\rangle_l$), Sugar and Biltonen[35] assumed that the location of the minimum between the two peaks of the bimodal distribution, i_{min}, separates the "small" clusters from the "large" ones (see Figure 1B) and applied the following equations:

$$\langle i\rangle_s = \frac{\sum_{i=1}^{i_{min}} i(iP_{all}(i))}{\sum_{i=1}^{i_{min}} iP_{all}(i)} \quad (1)$$

$$\langle i\rangle_l = \frac{\sum_{i=i_{min}+1}^{N} i(iP_{all}(i))}{\sum_{i=i_{min}+1}^{N} iP_{all}(i)} \quad (2)$$

where $iP(i)$ is the probability of randomly selecting a lattice point of a cluster of size i. From the unimodal distribution the average cluster size was calculated by means of eq 1, where $i_{min} = N$ was taken.

In the present work, when calculating the average cluster size, we could avoid the assumption that i_{min} separates the "small" clusters from the "large" ones, by constructing two separately collected size distributions: the size distribution of the largest clusters of the snapshots, $P_{la}(i)$, and the size distribution of all the other clusters of the snapshots, $P_{\bar{la}}(i)$. These two size distributions, $P_{la}(i)$ and $P_{\bar{la}}(i)$ (see Figure 1C), represent the deconvolution of the size distribution of all clusters, $P_{all}(i)$ (see Figure 1B). It is important to note that the $P_{la}(i)$ distribution coincides with the second peak of the bimodal distribution, $P_{all}(i)$, and thus the second peak refers to the size distribution of the largest cluster in each snapshot. By using $P_{la}(i)$ and $P_{\bar{la}}(i)$ distributions, we could calculate the average size of the largest, $\langle i\rangle_{la}$ and all the other clusters $\langle i\rangle_{\bar{la}}$, respectively, in the following way:

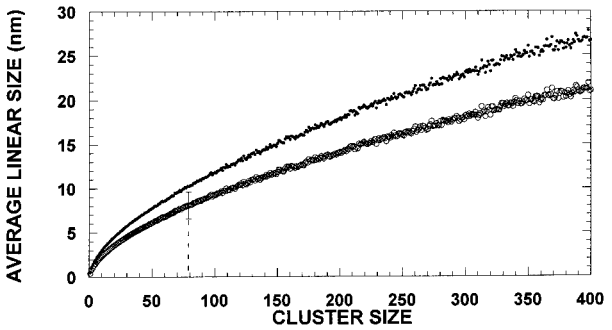

Figure 2. Calibration curves. Calculated average linear size, $\langle l\rangle$, of gel (open circle) and fluid clusters (closed circle) vs the cluster size. Each average was calculated after 90 000 Monte Carlo cycles. Dashed line shows the upper limit of the average size of the gel clusters (excluding the largest cluster of each snapshot) in equimolar DMPC/DSPC mixture. The estimation of the upper limit is based on the finite size scaling in Figure 6A.

$$\langle i\rangle_k = \frac{\sum_{i=1}^{N} i[iP_k(i)]}{\sum_{i=1}^{N} iP_k(i)} \quad (3)$$

where k = la or $\bar{la}$. As discussed before, the "large" clusters are practically equivalent to the largest cluster in each snapshot. Equations 1−3 define weighted averages, where the weight is proportional to the cluster size, i. These averages can be compared with measured cluster size averages if the probability of the cluster detection is proportional to the cluster size and also can be used as an estimate of the upper limit of the cluster size.

II.D. Calculating the Average Linear Size of the Clusters. We calculated the relationship between the cluster size (the number of acyl chains forming the cluster) and the respective average linear size. To calculate the linear size $l(i)$ of a cluster of size i, we determined first the lengths of the cluster perpendicular to the three characteristic directions of the triangular lattice [$l_1(i)$, $l_2(i)$, and $l_3(i)$] and then we selected the largest one of these lengths,

$$l(i) = \max\{l_1(i), l_2(i), l_3(i)\} \quad (4)$$

Depending on the shape of the clusters of size i, the linear size $l(i)$ can be different. In Figure 2 the calculated average of the linear size $\langle l(i)\rangle$ of fluid and gel clusters is plotted against the cluster size i. Calculating the linear size of gel and fluid clusters, we took the following interchain distances for nearest neighbor chains: $l_g = 0.48$ nm and $l_f = 0.61$ nm, respectively. The interchain distances were calculated from the cross sectional

area of a chain ($A_g = 0.20$ nm^2 in the gel and $A_f = 0.32$ nm^2 in the fluid state[36]) by using the following relationship:

$$l_k = \sqrt{\frac{2A_k}{\sqrt{3}}} \qquad \text{where} \qquad k = g \text{ or } f \tag{5}$$

II.E. Curves Fitted to the Simulated Data. The following sum of two sigmoid curves was fitted to the average size of the largest clusters $\langle i \rangle_{la}$ simulated at different temperatures, T:

$$\langle i \rangle_{la}(T) = \frac{A_f e^{a_f(T_1^f - T)}}{1 + e^{a_f(T_1^f - T)}} + \frac{B_f e^{b_f(T_2^f - T)}}{1 + e^{b_f(T_2^f - T)}} \tag{6}$$

for the fluid clusters and

$$\langle i \rangle_{la}(T) = \frac{A_g}{1 + e^{a_g(T_1^g - T)}} + \frac{B_g}{1 + e^{b_g(T_2^g - T)}} \tag{7}$$

for the gel clusters. A_j and B_j determine the height of each sigmoid curve, where j = g or f. T_1^j and $T_2^j (> T_1^j)$ are the temperatures at the inflection points of each sigmoid curve. The slopes at the first and second inflection points are $\pm A_j a_j/4$ and $\pm B_j b_j/4$, respectively, where the slope is positive for fluid and negative for gel clusters.

The following exponential function was fitted to the average cluster size $\langle i \rangle_{\bar{la}}$, simulated at different lattice sizes, N:

$$\langle i \rangle_{\bar{la}}(N) = \langle i \rangle_{\bar{la}}(\infty)(1 - e^{-\alpha N}) \tag{8}$$

where $\langle i \rangle_{\bar{la}}(\infty)$ (the average cluster size at infinite lattice) and α are model parameters.

III. Results and Discussion

Here the simulated cluster size distributions and cluster size averages are presented. There are only a limited number of experimental data available to directly support these calculations. The reason for this is that the size of the majority of the clusters is below the resolution of the currently available experimental techniques. For example, the linear size of the smallest gel cluster detectable by atomic force microscopy is 10 nm (personal communication with Dr. Kay Yee Lee, University of Chicago), while according to our calculations, most of the gel clusters are smaller than that. However, since DMPC/DSPC is the experimentally most intensively studied two-component lipid bilayer, we could test other model results against these available experimental data. The tests demonstrated that the model is able to predict the following macroscopic and microscopic membrane properties in agreement with the respective experimental data: the excess heat capacity curves at nine different mole fractions,[35] FRAP threshold temperatures at five different mole fractions,[31] the fractal dimension of gel clusters,[39] and the most frequent center-to-center distance of DSPC clusters at three different temperatures in equimolar mixture of DMPC/DSPC.[39] All these tests, though indirectly, support the cluster size distributions and averages calculated by using the same two-state model of DMPC/DSPC bilayer. A more direct comparison of the calculated cluster size distributions with the experimental data is discussed in the next section.

III.A. Cluster Size Distributions. If it is not stated otherwise, all simulations were performed on a triangular lattice of size 40×40, at three different DMPC/DSPC mole fractions of 30/70, 50/50, and 70/30, at several temperatures within the gel/fluid mixed phase region. Each simulation started with 6000 Monte Carlo cycles resulting in the equilibration of the system.

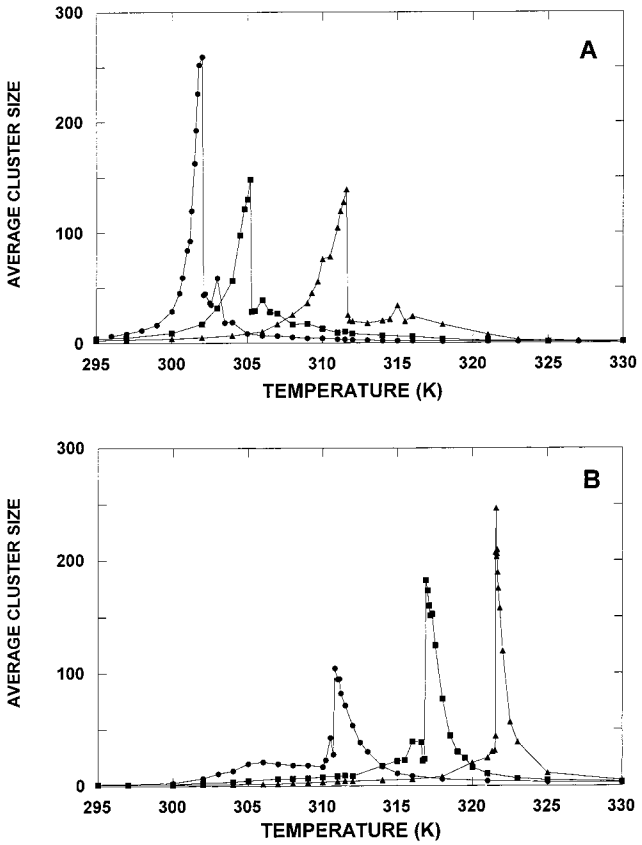

Figure 3. Average size of "small" clusters, $\langle i \rangle_s$, in DMPC/DSPC mixtures. (A) Average size of "small" fluid clusters vs temperature. (B) Average size of "small" gel clusters vs temperature. DMPC/DSPC mole fractions: 30/70 (triangle), 50/50 (square), 70/30 (circle). $\langle i \rangle_s$ is calculated by means of eq 1.

Then 6000 additional Monte Carlo cycles were performed. After the equilibrium was attained, the snapshots were analyzed at the end of each Monte Carlo cycle and the data were collected to generate the cluster size distributions. The size distributions of all the (gel or fluid) clusters, $P_{all}(i)$, were either unimodal or bimodal. The type of the distribution changes at the percolation threshold temperature of the clusters. The percolation threshold temperatures are listed for different DMPC/DSPC mole fractions in Table 4 of ref 31. In Figure 1A examples of unimodal and bimodal size distributions of fluid clusters in DMPC/DSPC (70/30) mixture are shown at three different temperatures. In the case of bimodal distribution, the cluster size at the minimum between the two peaks, i_{min}, marked by an arrow in Figure 1B, was assumed to separate the "small" from "large" fluid clusters.[35] The deconvolution of the bimodal distribution in Figure 1B is shown in Figure 1C, where $P_{la}(i)$ is the size distribution of the largest cluster of each snapshot and $P_{\bar{la}}(i)$ is the size distribution of all the other clusters of the snapshots. However, we should note that the distributions $P_{la}(i)$ and $P_{\bar{la}}(i)$ can be generated even if the respective $P_{all}(i)$ distribution is unimodal. When the size distribution of the clusters is bimodal, many small clusters coexist with one large cluster. The calculated upper bound to the size of the small gel clusters is 8 $\pm$ 1.5 nm (see section III.D). The average size of the largest gel cluster increases with decreasing temperature, and from the percolation threshold temperature it becomes comparable with the lattice size itself (see Figure 4B).

The size distribution of the clusters in DMPC/DSPC mixtures was not measured, but the following observations are consistent with a bimodal distribution. On one hand, neutron diffraction[21]

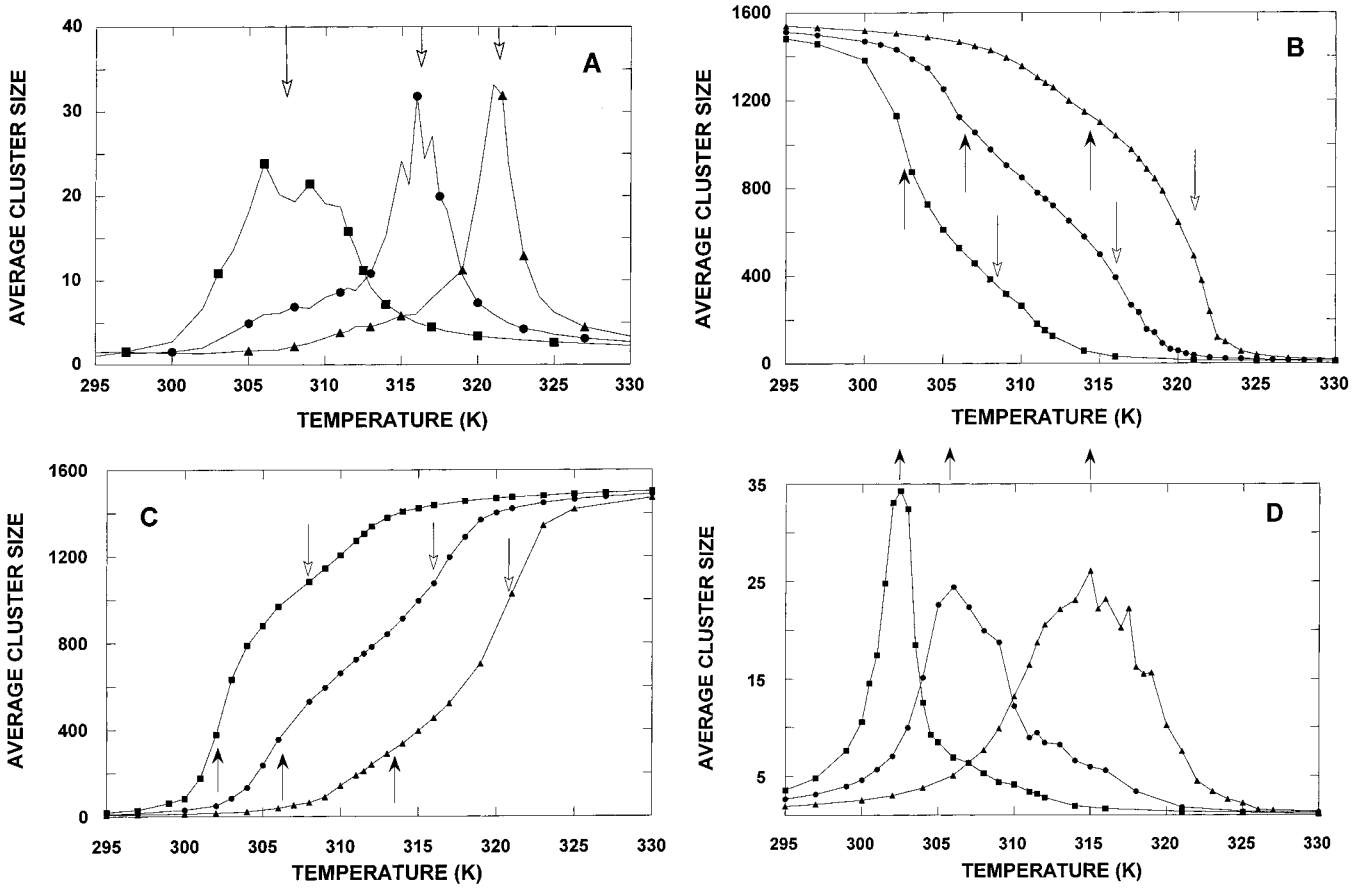

Figure 4. Temperature dependence of the average cluster sizes in DMPC/DSPC mixtures. (A) Average size of gel clusters, $\langle i \rangle_{\bar{la}}$ (excluding the largest cluster of each snapshot). (B) Average size of the largest gel cluster of each snapshot, $\langle i \rangle_{la}$. (C) Average size of the largest fluid cluster of each snapshot, $\langle i \rangle_{la}$. (D) Average size of fluid clusters, $\langle i \rangle_{la}^{-}$ (excluding the largest cluster of each snapshot). DMPC/DSPC mole fractions: 30/70 (triangle), 50/50 (circle), 70/30 (square). Arrows mark the maximum or inflection points of each curve. Averages are calculated by means of eq 3.

on equimolar DMPC/DSPC multilayers showed very small (<10 nm) DSPC clusters. [We note that in equimolar DMPC/DSPC bilayer the gel clusters are at most twice as large as the DSPC clusters because from the phase diagram[7] it follows that the mole fraction of DSPC in the gel clusters is larger than 0.5.] On the other hand, in similar conditions on GUV (of 30 μm diameter) a gel cluster (or a small number of gel clusters) of size comparable with the vesicle surface was visible in the gel−fluid mixed phase region by fluorescent microscopy[22] and its size increased with decreasing temperature.

III.B. Cluster Size Averages. The temperature dependence of the average size of the "small" fluid and gel clusters for DMPC/DSPC compositions of 30/70, 50/50, and 70/30 is shown in Figure 3A,B. The averages were calculated by means of eq 1. Each curve has a sharp maximum and at certain mixing ratios a small broad peak can be recognized, too. The broad peak is very clearly expressed in the case of fluid clusters at mixing ratio 30/70 (Figure 3A) and in the case of gel clusters at 70/30 (Figure 3B). To understand this nontrivial temperature dependence of the average size of "small" clusters $\langle i \rangle_s$, we created the size distribution of the largest cluster of each snapshot, $P_{la}(i)$, and the size distribution of all the other clusters, $P_{la}^{-}(i)$, and calculated the respective cluster size averages $\langle i \rangle_{la}$ and $\langle i \rangle_{\bar{la}}$ by using eq 3. The temperature dependence of $\langle i \rangle_{la}$ in Figure 4B,C can be represented as a sum of two sigmoid curves given by eqs 6 and 7, for the fluid clusters and for the gel clusters, respectively. The upward and downward arrows in Figure 4B,C mark the inflection points of the $\langle i \rangle_{la}$ curves. The parameters of the fitted double sigmoid curves are listed in Table 1. The temperature dependence of $\langle i \rangle_{la}^{-}$ is shown in Figure 4A,D, where the maximum of each curve is marked by upward and downward arrows for fluid and gel clusters, respectively. It is important to note the following observations: (i) The

Table 1[a]

	DMPC/DSPC mole fraction		
	70/30	50/50	30/70
A_f	643.19 ± 29.44	711.27 ± 25.30	611.25 ± 50.43
A_g	813.34 ± 57.42	767.44 ± 30.31	811.29 ± 65.86
B_f	849.40 ± 29.77	766.82 ± 28.50	856.62 ± 51.72
B_g	658.34 ± 56.83	743.07 ± 25.45	716.27 ± 63.20
a_f (K^{-1})	−1.454 ± 0.103	−0.593 ± 0.031	−0.365 ± 0.023
a_g (K^{-1})	−1.023 ± 0.083	−0.489 ± 0.030	−0.307 ± 0.021
b_f (K^{-1})	−0.325 ± 0.008	−0.527 ± 0.031	−0.826 ± 0.057
b_g (K^{-1})	−0.435 ± 0.037	−0.603 ± 0.027	−1.176 ± 0.136
T_1^f (K)	302.26 ± 0.04	306.28 ± 0.16	313.37 ± 0.49
T_1^g (K)	302.39 ± 0.08	306.00 ± 0.33	314.33 ± 0.54
T_2^f (K)	307.69 ± 0.22	315.95 ± 0.15	320.82 ± 0.09
T_2^g (K)	308.83 ± 0.45	316.00 ± 0.13	321.03 ± 0.07
T_{max}^f (K)	302.40 ± 0.20	305.80 ± 0.60	314.80 ± 0.30
T_{max}^g (K)	307.00 ± 2.00	316.00 ± 0.30	321.00 ± 0.50
T_{DMPC} (K)	302.65 ± 0.15	306.73 ± 0.15	313.57 ± 0.32
T_{DSPC} (K)	308.46 ± 0.14	314.86 ± 0.24	320.32 ± 0.38
r_f	0.999 88	0.999 77	0.999 85
r_g	0.999 82	0.999 77	0.999 51

[a] A_j and B_j are the heights of the first and second sigmoids. $\pm a_j A_j/4$ and $\pm b_j B_j/4$ are the slopes of the first and second sigmoids at their inflection points at T_1^j and T_2^j ($T_1^j < T_2^j$ and j = g or f), respectively, and the slope is positive for fluid and negative for gel clusters. T_{max}^i is the temperature at the maximum of the average cluster size $\langle i \rangle_{la}^{-}(T)$. T_{DMPC} and T_{DSPC} are the temperatures at the inflection points of the melting curves of the individual components of the DMPC/DSPC mixtures. r_j is the correlation coefficient for the fit of the double sigmoid curve.

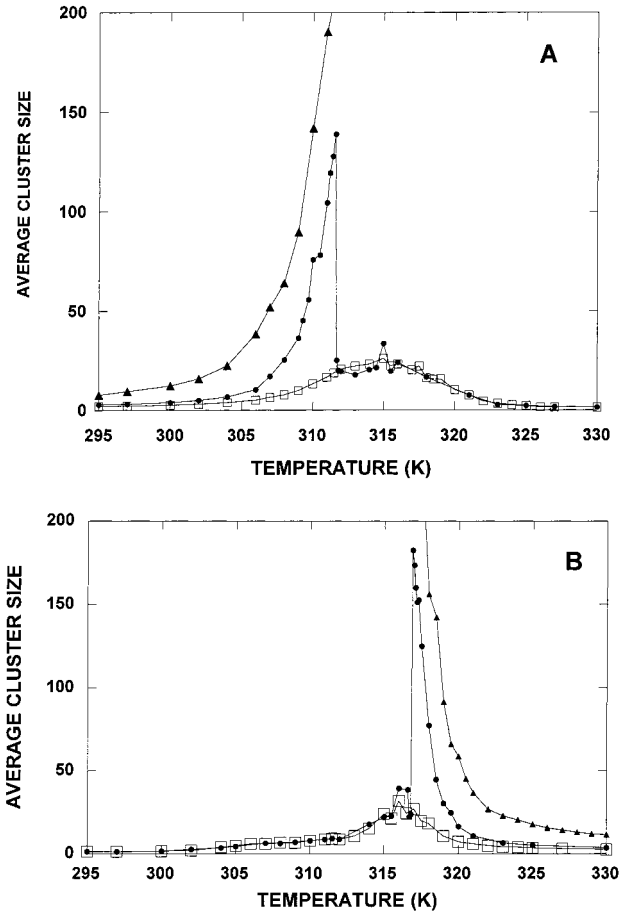

Figure 5. Comparison of three different cluster size averages, $\langle i\rangle_s(T)$, $\langle i\rangle_{la}(T)$, and $\langle i\rangle_{\bar{la}}(T)$. (A) Average sizes of fluid clusters vs temperature. DMPC/DSPC mole fraction is 30/70. (B) Average sizes of gel clusters vs temperature. DMPC/DSPC mole fraction is 50/50. Key: circle, average size of the "small" clusters, $\langle i\rangle_s(T)$; triangle, average size of the largest cluster of each snapshot, $\langle i\rangle_{la}(T)$; open square, average size of all the clusters except the largest ones, $\langle i\rangle_{\bar{la}}(T)$.

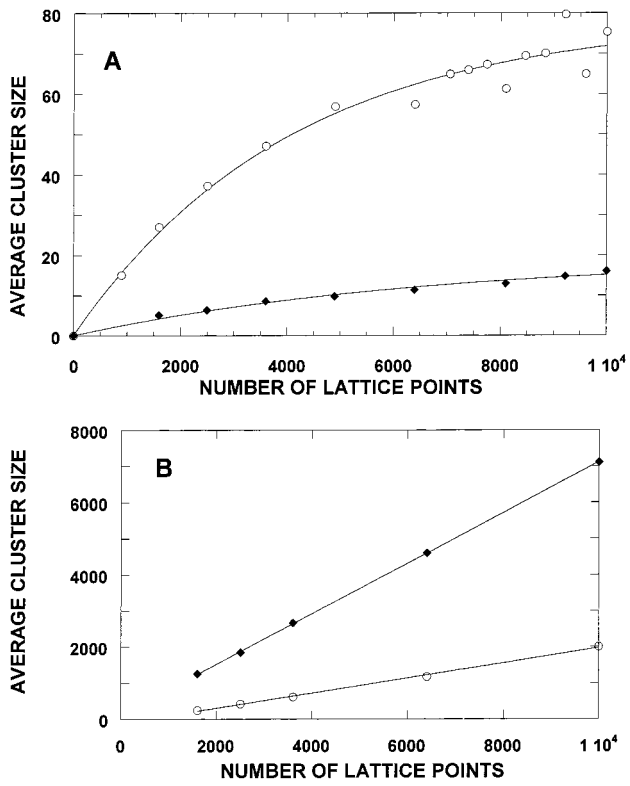

Figure 6. Finite size scaling. (A) Average size of all the gel clusters (except the largest one of each snapshot) vs lattice size, N. Equation 8 is fitted to the calculated data. The parameters of the fitted curves are $\langle i\rangle_{\bar{la}}(\infty) = 78.4 \pm 3.8$ for 317 K and $\langle i\rangle_{\bar{la}}(\infty) = 19.5 \pm 1.9$ for 305 K, while $\alpha = (25 \pm 3) \times 10^{-5}$ for 317 K and $\alpha = (15 \pm 3) \times 10^{-5}$ for 305 K. The correlation coefficients are: 0.986 and 0.993 for 317 and 305 K, respectively. (B) Average size of the largest gel cluster of each snapshot vs lattice size. Straight lines are fitted to the data points (solid line). The slopes of the fitted lines are 0.208 ± 0.005 and 0.699 ± 0.003 at 317 and 305 K, respectively. The intercepts of the fitted lines are -10 ± 31 and 121 ± 18 at 317 and 305 K, respectively. The correlation coefficients are 0.9989 and 0.99997 for 317 and 305 K, respectively. Key: circle, 317 K; diamond, 305 K. The DMPC/DSPC mole fraction is 50/50.

locations of the inflection points of the $\langle i\rangle_{la}(T)$ curves correspond to the maximum of the $\langle i\rangle_{\bar{la}}(T)$ curves. (ii) The two composing sigmoid curves can be compared to the calculated melting curves of the individual components in different DMPC/DSPC mixtures (see Figure 3 in ref 31). The melting curves of the individual components can be described by single sigmoid curves, and their inflection points, listed in Table 1, coincide with the inflection points of the double sigmoid curves in Figure 4B,C. (iii) One can also notice that $T_1^g \approx T_1^f$ and $T_2^g \approx T_2^f$. All these coincidences show that the first inflection point in the curves of Figure 4B,C can be associated with the melting of the acyl chains of the DMPC molecules, while the second inflection point can be associated with the melting of the acyl chains of the DSPC molecules. It follows from coincidence (i) that the rate of association of the fluid clusters to the largest fluid cluster is maximal at the first inflection point, while the rate of association of the gel clusters to the largest gel cluster is maximal at the second inflection point.

III.C. Temperature-Induced Cluster Formation in DMPC/DSPC Mixtures. The comparison of $\langle i\rangle_{la}(T)$ and $\langle i\rangle_{\bar{la}}(T)$ curves with the respective $\langle i\rangle_s(T)$ curve gives a clear interpretation of the peaks in the $\langle i\rangle_s(T)$ curve. In Figure 5A $\langle i\rangle_{la}$, $\langle i\rangle_{\bar{la}}$, and $\langle i\rangle_s$ cluster size averages of the fluid clusters in DMPC/DSPC (30/70) mixture are plotted against the temperature and marked by a closed triangle, open square, and closed circle, respectively. Since the small broad peak of the $\langle i\rangle_s$ curve coincides with the $\langle i\rangle_{\bar{la}}$ curve it refers to the average size of all the clusters except the largest one. One can also notice that the left edge of the sharp peak of the $\langle i\rangle_s$ curve and the $\langle i\rangle_{la}$ curve show very similar increases with increasing temperature. Thus, up to 312 K the sharp peak of the $\langle i\rangle_s$ curve refers to the average size of the largest clusters in the snapshots. Note that in this temperature range $\langle i\rangle_s$ is slightly smaller than $\langle i\rangle_{la}$ because $\langle i\rangle_s$ is an average over all the clusters, while $\langle i\rangle_{la}$ is an average over the largest clusters only. Figure 5B represents the average size of the gel clusters at equimolar DMPC/DSPC mixture. In this case the small broad peak (marked by open squares) and the sharp large peak of $\langle i\rangle_s(T)$ curve overlap each other.

By means of the above rationalization of the $\langle i\rangle_s(T)$ curves in Figure 5A, one can qualitatively describe the temperature-induced formation of the fluid clusters in the DMPC/DSPC (30/70) mixture. From the calorimetric onset temperature of the gel-to-fluid transition,[31] 300 K, the size of the largest fluid cluster grows with an increasing rate, while the number of clusters does not change considerably (see Figure 4B in ref 39). The growth of the largest fluid cluster is the result of the association with nearby growing fluid clusters. First, this is a loose and rather dynamic network of clusters, but with increasing temperature it becomes a stronger and more static association of clusters. At about the percolation threshold temperature of the fluid clusters,[31] 313.1 K, the unimodal size distribution function

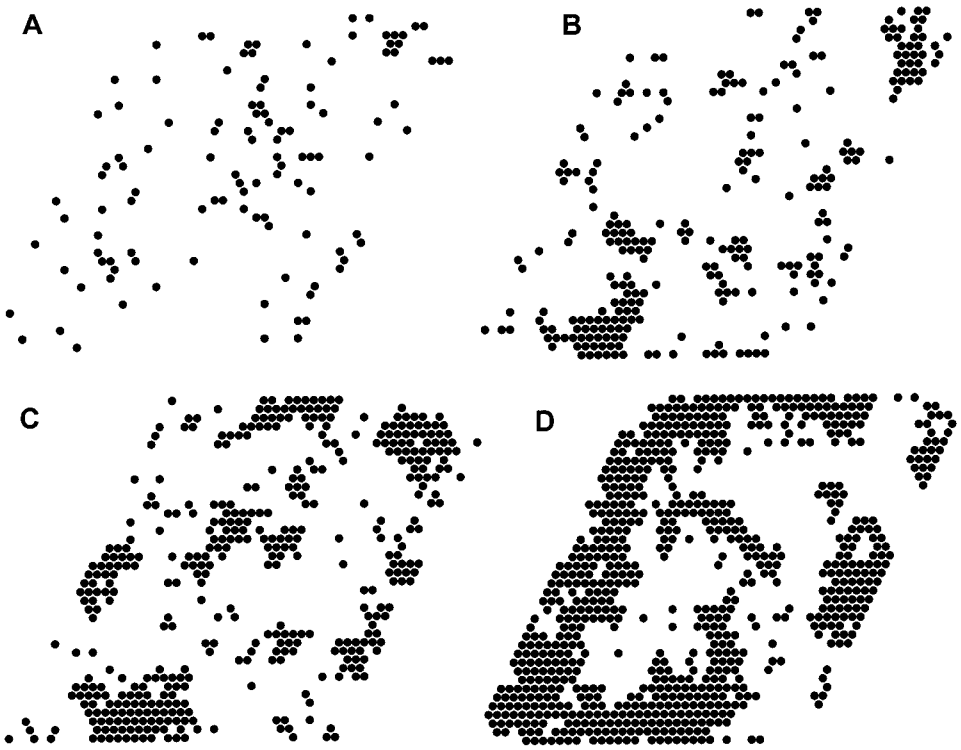

Figure 7. Process of cluster formation. Formation of gel clusters are shown immediately after quenching an equimolar mixture of DMPC/DSPC from 400 to 313 K. Snapshots of the gel clusters were taken after the following number of Monte Carlo cycles: (A) 1, (B) 5, (C) 10, (D) 500. The conditions of the simulation are described in the text. Dot: hydrocarbon chain in gel state.

becomes bimodal, and once this happens, the clusters larger than i_{min} are excluded from the calculation of $\langle i \rangle_s$ (see section II.C and eq 1). For this reason the average size of the "small" clusters $\langle i \rangle_s$ drops to about 25 (the height of the smaller peak in Figure 5A). This is about the size of the larger clusters among the "small" ones. These larger clusters are separated from the largest fluid cluster and from each other such that they are unable to associate. Any further increase of the temperature increases slightly the size of these larger clusters because of the melting of nearby chains and association with smaller clusters. From about 315 K, however, the increasing larger clusters get closer to the similarly increasing largest cluster. When the larger among the "small" clusters begin to associate with the largest fluid cluster, the average size of the remaining "small" clusters starts to decrease.

III.D. Linear Size of Gel Clusters and Finite Size Scaling. In Figure 2 the calculated average linear size, $\langle l(i) \rangle$ of gel and fluid clusters is plotted against the cluster size, i. These calibration curves were calculated from a simulation of the equimolar DMPC/DSPC mixture at 305.3 K. Practically the same calibration curves were obtained for simulations at other temperatures and mole fractions within the gel/fluid mixed phase region. In an equimolar mixture of DMPC/DSPC the average size of the gel clusters $\langle i \rangle_{\bar{la}}$ is less than 31 acyl chains (see Figure 4A). Thus, according to the calibration curve in Figure 2, the average linear size of the gel clusters, $\langle i \rangle_{\bar{la}}$ is less than 4.5 ± 0.8 nm. Since the size of the lattice, 40×40, is several orders of magnitude smaller than the size of the real bilayer, it is important to investigate how $\langle i \rangle_{\bar{la}}$ and $\langle i \rangle_{la}$ depend on the lattice size. [Note that the excess heat capacity of equimolar DMPC/DSPC mixture does not change significantly from a critical lattice size[31] of 20×20.] Thus, additional simulations of the equimolar DMPC/DSPC mixtures were performed in a triangular lattice of size 50×50, 60×60, 70×70, 80×80, 90×90, 96×96, and 100×100, at 305 and 317 K. Each simulation started with 6000 equilibration Monte Carlo cycles, while the number of the additional Monte Carlo cycles increased with the lattice size. The temperature 317 K was chosen because the average size of the gel clusters, $\langle i \rangle_{\bar{la}}$, is maximal at this temperature (see the middle curve in Figure 4A). In Figure 6A the calculated average size of the gel clusters, $\langle i \rangle_{\bar{la}}$ is plotted against the number of lattice points, N. An exponential function given by eq 8 can be nicely fitted to the calculated points in Figure 6A. The nonlinear parameter estimation results in the average size of the gel clusters at infinite lattice size ($\langle i \rangle_{\bar{la}}(\infty) = 78.4 \pm 3.8$ for 317 K and $\langle i \rangle_{\bar{la}}(\infty) = 19.5 \pm 1.9$ for 305 K), while $\alpha = 25 \pm 3 \times 10^{-5}$ for 317 K and $\alpha = 15 \pm 3 \times 10^{-5}$ for 305 K. Finally, by using the above $\langle i \rangle_{\bar{la}}(\infty)$ values and the calibration curve for gel clusters in Figure 2, one can obtain the following average linear sizes for the gel clusters: 8.06 ± 1.54 and 3.4 ± 0.6 nm for 317 and 305 K, respectively. Thus, the average size of the gel clusters in the transition region of equimolar DMPC/DSPC mixture, calculated for infinite lattice size, is less than 8.06 ± 1.54 nm. This calculated upper bound for the linear size of the small gel clusters is close to 10 nm, the estimation of Gliss et al.[21] derived from neutron diffraction and AFM data. While the size of all the clusters, except the largest one in each snapshot, remains small, the size of the largest clusters increases with increasing lattice size (see Figure 6B). One or a small number of large gel clusters in an unsupported giant unilamellar vesicle of equimolar DMPC/DSPC were recently visualized by means of fluorescence microscopy.[22] The sizes of these clusters were comparable with the vesicle's size. We strongly believe that the large cluster visualized by fluorescence microscopy is equivalent to the large cluster predicted from the bimodal equilibrium distribution of the cluster size (Figure 1A). More than one large cluster can be observed if the lateral distribution of the lipid molecules in the giant vesicle does not attain equilibrium (see Appendix). One

may accelerate the attainment of the equilibrium by means of freezing and thawing cycles.[37]

IV. Conclusions

A simple two-component, two-state lattice model is sufficient to simulate the excess heat capacity curves, percolation threshold temperatures, most frequent center-to-center distances of DSPC clusters, fractal dimensions of gel clusters, and the upper bound of the size of the nonpercolated gel clusters of DMPC/DSPC bilayers in quantitative agreement with the experimental data. Below the percolation threshold temperature the calculated unimodal size distribution of gel clusters becomes bimodal; i.e., small nanometer-size clusters coexist with a cluster of size comparable with the bilayer's surface area. The size of the large gel cluster increases with decreasing temperature, while the average size of the small clusters remains less than 8 nm and has a local maximum at the percolation threshold temperature. These predictions of the model are in qualitative agreement with the neutron diffraction and fluorescent microscopy data. The increase of the large gel cluster with decreasing temperature takes place in two steps: the higher and lower temperature step is associated with the fluid-to-gel transition of DSPC and DMPC molecules, respectively. The rate of association of the gel clusters to the large gel cluster is maximal at the high-temperature step, while the rate of association of the fluid clusters to the large fluid cluster is maximal at the lower temperature step.

V. Appendix

In Figure 7 the attainment of the equilibrium is shown through a series of snapshots in the case of equimolar DMPC/DSPC mixture. The simulation started with 2000 Monte Carlo cycles at high temperature (400 K) in order to attain random distribution of the components and the orientation of the molecules. Then the temperature was suddenly decreased to 313 K, where the equilibrium size distribution of gel clusters is bimodal. Then snapshots, shown in Figure 7, were taken after certain number of Monte Carlo cycles. Within each Monte Carlo cycle, $2N$ local state alterations were followed by $4N/3$ orientation changes (where N is the lattice size, $N = 1600$). Only these physically realistic trial state generating steps were taken in order to give a realistic picture about the process of gel cluster formation and an idea about the change of the cluster size distribution from nonequilibrium to equilibrium distribution. The snapshots show that initially only randomly distributed small clusters are present (see Figure 7A), then growing of the existing clusters takes place and new small clusters appear. There are several larger and smaller clusters simultaneously present (see Figure 7B,C), while after hundreds of Monte Carlo cycles one large cluster and many, much smaller ones are present in the snapshot (see Figure 7D; note that because of the periodic boundary conditions the clusters along the edge of the lattice are connected, forming one large cluster).

Acknowledgment. I.P.S. is grateful for Mrs. Lawrence Garner's generous support. This work was also supported by Pfizer, Inc.

References and Notes

(1) Toccane, J. F. *Comm. Mol. Cell. Biophys.* **1992**, *8*, 53−72.

(2) Bergelson, L. O.; Garwish, K.; Feretti, J. A.; Blumenthal, R. *Mol. Membr. Biol.* **1995**, *12*, 1−162.

(3) Glaser, M.; Wanaski, W. S.; Buser, C. A.; Boguslavsky, V.; Rashidzada, W.; Morris, A.; Rebecci, M.; Scarlata, S. F.; Runnels, L. W.; Prestwich, G. D.; Chen, J.; Aderem, A.; Ahn, J.; McLaughlin, S. *J. Biol. Chem.* **1996**, *271*, 26187−26193.

(4) Yang, L. G. M. *Biochemistry* **1996**, *35*, 13966−13974.

(5) Welby, M. P. Y.; Tocanne, J. F. *FEBS Lett.* **1996**, *384*, 107−111.

(6) Norris, V.; Madsen, M. S. *J. Mol. Biol.* **1995**, *253*, 739−748.

(7) Mabrey, S.; Sturtevant, J. M. *Proc. Natl. Acad. Sci. U.S.A.* **1976**, *73*, 3862−3866.

(8) Van Dijck, P. W. M.; Karper, A. J.; Oonk, H. A. J.; De Gier, J. *Biochim. Biophys. Acta* **1977**, *470*, 58−69.

(9) Wilkinson, D. A.; Nagle, J. F. *Biochemistry* **1979**, *18*, 4244−4249.

(10) Knoll, W.; Ibel, K.; Sackmann, E. *Biochemistry* **1981**, *20*, 6379−6383.

(11) Lu, D.; Vavasour, I.; Morrow, M. R. *Biophys. J.* **1995**, *68*, 574−583.

(12) Sankaram, M. B.; Thompson, T. E. *Biochemistry* **1992**, *31*, 8258−8268.

(13) Sankaram, M. B.; Marsh, D.; Thompson, T. E. *Biophys. J.* **1992**, *63*, 340−349.

(14) Mendelsohn, R.; Maisano, J. *Biochim. Biophys. Acta* **1978**, *506*, 192−201.

(15) Brumm, T, J. K.; Mouritsen, O. G.; Bayerl, T. *Biophys. J.* **1996**, *70*, 1373−1379.

(16) Vaz, W. L. C.; Melo, E. C. C.; Thompson, T. E. *Biophys. J.* **1989**, *56*, 869−876.

(17) Schram, V.; Lin, H.-N.; Thompson, T. E. *Biophys. J.* **1996**, *71*, 1811−1822.

(18) Piknova, B.; Marsh, D.; Thompson, T. E. *Biophys. J.* **1996**, *71*, 892−897.

(19) Von Dreele, P. H. *Biochemistry* **1978**, *17*, 3939−3943.

(20) Pedersen, S.; Jorgensen, K.; Bækmark, T.; Mouritsen, O. G. *Biophys. J.* **1996**, *71*, 554−560.

(21) Gliss, C.; Clausen-Schaumann, H.; Gunther, R.; Odenbach, S.; Randl, O.; Bayerl, T. M. *Biophys. J.* **1998**, *74*, 2443−50.

(22) Bagatolli, L. A.; Gratton, E. *Biophys. J.* **2000**, *78*, 290−305.

(23) Ipsen, J. H.; Mouritsen, O. G. *Biochim. Biophys. Acta* **1988**, *944*, 121−134.

(24) Brumbaugh, E. E.; Johnson, M.; Huang, C. *Chem. Phys. Lipids* **1990**, *52*, 69−78.

(25) Brumbaugh, E. E.; Huang, C. *Methods Enzymol.* **1992**, *210*, 521−539.

(26) Priest, R. *Mol. Cryst. Liq. Cryst.* **1980**, *60*, 167−184.

(27) Sugar, I. P.; Monticelli, G. *Biophys. J.* **1985**, *48*, 283−288.

(28) Jan, N.; Lookman, T.; Pink, D. *Biochemistry* **1984**, *23*, 3227−3231.

(29) Jørgensen, K.; Sperotto, M.; Mouritsen, O. G.; Ipsen, J.; Zuckermann, M. *Biochim. Biophys. Acta* **1993**, *1152*, 135−142.

(30) Risbo, J.; Sperotto, M.; Mouritsen, O. G. *J. Chem. Phys.* **1995**, *103*, 3643−3656.

(31) Sugar, I. P.; Thompson, T. E.; Biltonen, R. L. *Biophys. J.* **1999**, *76*, 2099−2110.

(32) Huang, K. *Statistical Mechanics*; Wiley: New York, 1963; p 336.

(33) Metropolis, M.; Rosenbluth, A. W.; Rosenbluth, M. N.; Teller, A. N. *J. Chem. Phys.* **1953**, *21*, 1087−1092.

(34) Sun, H.; Sugar, I. P. *J. Phys. Chem.* **1997**, *101*, 3221−3227.

(35) Sugar, I. P.; Biltonen, R. L. *Methods. Enzymol.* **2000**, *323*, 340−372.

(36) Nagle, J. F.; Zhang, R.; Tristram-Nagle, S.; Sun, W.; Petrache, H. I.; Suter, R. M. *Biophys. J.* **1996**, *70*, 1419−1431.

(37) Liu, F.; Sugar, I. P.; Chong, P. L.-G. *Biophys. J.* **1997**, *72*, 2243−2254.

(38) Sonnleitner, A.; Schutz, G. J.; Schmidt, Th. *Biophys. J.* **1999**, *77*, 2638−2642.

(39) Sugar, I. P.; Michonova-Alexova, E.; Chong, P. L.-G. *Biophys. J.* **2001**, in press.

(40) Binder, K.; Stauffer, D. Monte Carlo studies of "random" systems. In *Applications of the Monte Carlo Method in Statistical Physics*; Binder, K., Ed.; Springer-Verlag: Berlin, Heidelberg, New York, Tokyo, 1987; Chapter 8.